Kinetic Model for Surfactant-Induced Pore Wetting in Membrane Distillation

Zhangxin Wang, Yuanmiaoliang Chen, Shihong Lin

www.elsevier.com/locate/memsci

PII: S0376-7388(18)31062-7
DOI: https://doi.org/10.1016/j.memsci.2018.07.010
Reference: MEMSCI16289

To appear in: *Journal of Membrane Science*

Received date: 18 April 2018
Revised date: 8 June 2018
Accepted date: 5 July 2018

Cite this article as: Zhangxin Wang, Yuanmiaoliang Chen and Shihong Lin, Kinetic Model for Surfactant-Induced Pore Wetting in Membrane Distillation, *Journal of Membrane Science,* https://doi.org/10.1016/j.memsci.2018.07.010

Kinetic Model for Surfactant-Induced Pore Wetting in Membrane Distillation

Zhangxin Wang[a], Yuanmiaoliang Chen[a], and Shihong Lin[a],[b]*

[a]Department of Civil and Environmental Engineering, Vanderbilt University, Nashville, Tennessee 37235-1831, United States
[b]Department of Chemical and Biomolecular Engineering, Vanderbilt University, Nashville, Tennessee 37235-1831, United States

Corresponding author: email: shihong.lin@vanderbilt.edu; Tel. +1(615)322-7226

ABSTRACT

Membrane pore wetting is a unique and important technical challenge for membrane distillation (MD). While the general principle of pore wetting is well known, the detailed mechanism of pore wetting induced by surfactants that can actively adsorb onto membrane pore surface has not been theoretically elucidated. In this study, we developed a theoretical model, based on surfactant transport in a partially wetted membrane pore under the pseudo-steady state assumption, to quantify the kinetics of pore wetting. The theoretical model predicts several key dependences of wetting kinetics on operating parameters and solution properties, which are highly consistent with results from MD experiments using feed solution containing sodium dodecyl sulfate. It was found that kinetics of pore wetting is strongly dependent on vapor flux, surfactant concentration, but relatively independent of the transmembrane hydraulic pressure. The critical surfactant concentration below which pore wetting does not occur was also predicted by the wetting model. Finally, impact of surfactant species on wetting kinetics was also discussed.

Nomenclature

B	geometric factor accounting for non-cylindrical pore geometry (dimensionless)
c	surfactant concentration (mM)
c^*	critical surfactant concentration at the frontier to satisfy ΔP=LEP (mM)
c_0	surfactant concentration in the bulk solution (mM)
c_0'	critical (minimum) bulk surfactant concentration to induce wetting (mM)
c^*_{max}	maximum c^* beyond which wetting does not occur (mM)
D	diffusion coefficient of surfactant (m^2 s^{-1})
J_w	water vapor flux (L m^2 hr^{-1})
K	equilibrium constant of surfactant adsorption on PVDF surface (mM^{-1})
LEP	liquid entry pressure (kPa)
l	wetting length: depth of the partially wetted portion of the pore (μm)
ΔP	transmembrane hydraulic pressure (kPa)
R	membrane pore radius (μm)
$t_{wetting}$	breakthrough time (min)
γ_L	surface tension of the solution (mN/m)
δ_b	thickness of the boundary layer (μm)
δ_m	membrane thickness (μm)
ε	membrane porosity (dimensionless)
θ	intrinsic contact angle (º)
τ	surface adsorption density of surfactants (mmole m^{-2})
τ_{max}	maximum surface adsorption density of surfactants (mmole m^{-2})

1. Introduction

Membrane distillation (MD) is a membrane-based thermal desalination technology [1–3]. In a typical MD process, a microporous hydrophobic membrane is employed to separate a hot salty stream (the feed solution) and a cold salt-free distillate stream. Driven by the partial vapor pressure difference resulting from the temperature difference between the feed and distillate streams, water vapor transports through the membrane pores from the feed stream to the distillate stream. Any non-volatile solute (e.g. salt) is rejected by the hydrophobic membrane. Compared to reverse osmosis (RO), the state-of-the-art desalination technology, MD has several advantages

including the capability of treating hypersaline brines, the ability to utilize low grade thermal energy, relatively low capital cost due to the absence of high pressure and high temperature components, and small system footprint that is important to mobile desalination applications[4–13].

However, large scale practical applications of MD are still limited due to a variety of technical challenges, several of which are related to the use of conventional hydrophobic membranes. In particular, membrane pore wetting is an important technical challenge that is unique to MD (i.e. it does not exist in other membrane processes) [14–17]. Membrane pore wetting refers to the penetration of feed solution through membrane pores, which in most cases leads to unacceptable salt rejection. Membrane pore wetting can be induced by low-surface-tension liquids (e.g. alcohol), amphiphilic molecules (e.g. surfactants), or other natural surface active agents [18–21]. Much effort has been made on developing novel membrane materials and operating strategies to prevent or mitigate pore wetting in MD, which includes the development of omniphobic membranes [20,22–24], composite membranes with a hydrophilic surface layer [25,26], and superhydrophobic membrane coupled with air-layer recharging during operation [19,27].

Interestingly, despite the technological successes in developing wetting prevention measures, the exact mechanism of pore wetting in MD has not been fully understood. Most past studies applied the very simple wetting criterion based on comparing transmembrane pressure and liquid entry pressure [3,28,29]. Some recent studies suggested amphiphilic contaminants can render the membrane surface hydrophilic and thereby induce wetting [30,31]. In a recent study, we showed the fundamental difference between pore wetting induced by alcohol, with which the impact of surface adsorption is negligible, and by surfactants, with which the impact of surface adsorption is significant[32]. It was shown that alcohol-induced wetting was instantaneous whereas surfactant-induced wetting was progressive[33,34]. Our study also suggests that, while the presence of surfactants in feed solution promotes wetting, the adsorption of surfactants onto pore surface does not promote wetting by rendering the pores hydrophilic, but instead deters pore wetting by reducing the surface tension of the feed solution at the liquid-air interface [32]. To accurately describe the kinetics of surfactant-induced wetting, we need to develop a model that accounts for all major mechanisms for mass transport of surfactants into the membrane pores, which has never been reported in literature.

In this study, we investigate the kinetics of pore wetting in MD with feed solutions containing surfactants. We first develop a theoretical model to predict the kinetic rate of wetting frontier propagation in a progressively wetted membrane pore. This model is based on three major assumptions including force equilibrium at the liquid-air interface, pseudo-steady state transport of surfactants, and pseudo-equilibrium surfactant adsorption. This kinetic model accounts for the major transport mechanisms of convection, diffusion, and adsorption of surfactants in a slowly expanding volume of feed solution in a partially wetted pore. We use sodium dodecyl sulfate (SDS) as a model surfactant to validate several key characteristics predicted by the model, and then use the model to extend the analysis for more operating conditions and other types of surfactants.

2. Theory and model development

The widely accepted wetting criterion in an MD process is that the transmembrane hydraulic pressure (ΔP) exceeds the liquid entry pressure, LEP, of the membrane pore (Eq. 1)[35–37].

$$\Delta P \geq LEP \tag{1}$$

By definition, LEP is the minimum pressure for a liquid to enter a pore and can be calculated using with Eq. 2.

$$LEP = -\frac{2B\gamma_L \cos\theta}{R} \tag{2}$$

where γ_L is the surface tension of the feed solution, θ is the intrinsic contact angle between the feed solution and the membrane surface, R is the equivalent radius of the membrane pore, B is the geometric factor accounting for the non-cylindrical pore geometry ($B = 1$ for cylindrical pore). The presence of surfactants (e.g. SDS) in an aqueous solution reduces both γ_L and $\cos\theta$ in Eq. 2 and thereby results in a decreased LEP [18,22,38,39]. The LEP decreases as the surfactant concentration increases. We note that transmembrane hydraulic pressure, instead of just the hydraulic pressure of the feed stream, should be used in Eq. 1. This is rather counter-intuitive but has been thoroughly explained by Zmievskii [37].

If the SDS concentration in the feed solution is sufficiently high (Fig. 1(a)), the corresponding LEP would be lower than ΔP, and the feed solution would enter the membrane pore according to the wetting criterion. As the feed solution intrudes into the membrane pore, the SDS in the feed solution would adsorb onto the hydrophobic surface in the membrane pore. The adsorption causes a decrease of SDS concentration at the wetting frontier and consequently leads to an increased LEP (calculated based on the reduced frontier SDS concentration), which impedes the further progression of wetting frontier in the membrane pore. With the supplement of SDS to the wetting frontier by convection induced by vapor flux and diffusion induced by concentration gradient, the SDS concentration in the wetting frontier could be maintained at a critical concentration (c^*) if force equilibrium at the liquid-air interface (i.e. LEP=ΔP at the wetting frontier) is assumed. This force balance assumption is reasonable because a hypothetic Hagan-Poiseuille flow of a force unbalanced water column would take only a fraction of a second to penetrate the pores, which is significantly faster than what have been observed. The force equilibrium at the wetting frontier can be maintained until the SDS concentration at the wetting frontier has to increase beyond c^* when SDS can no longer adsorb onto the pore surface near the wetting frontier due to surface saturation. Because the surface tension of the feed solution at the wetting frontier, which is dependent on c^*, and the surface tension of the unwetted pore surface, which is relevant to LEP calculation, are both constant, the static contact angle at the triple phase boundary at the wetting frontier can also be approximated to be constant.

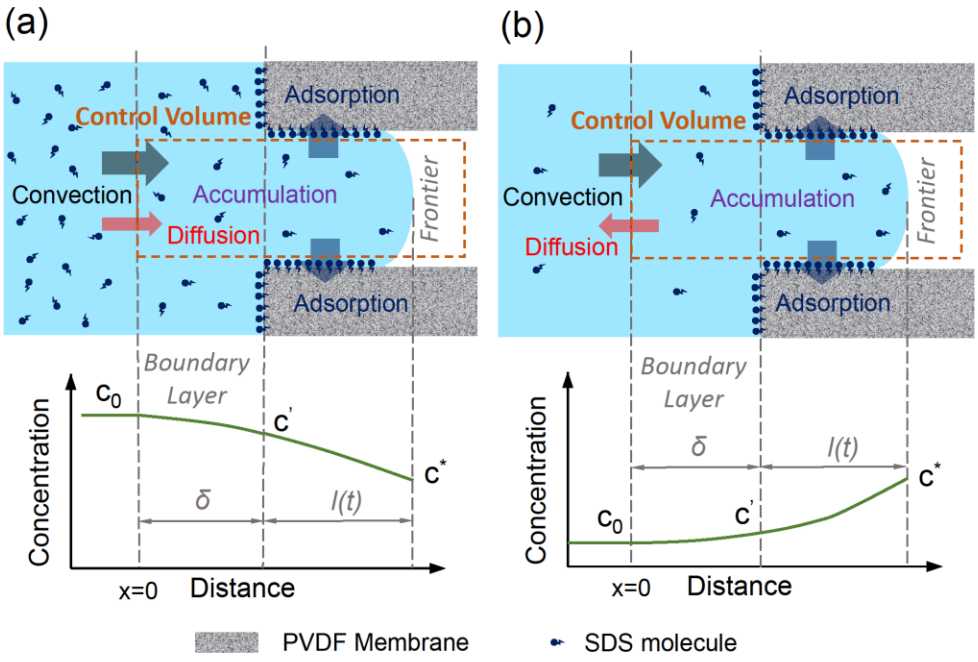

Fig. 1. Schematics of a cylindrical pore wetting by SDS at (a) a high concentration and (b) low concentration, respectively. In both scenarios, for the SDS solution to enter the membrane pore, the SDS concentration in the solution frontier must reach the critical concentration c^* (corresponding to LEP=ΔP). Once the SDS solution enters the membrane pore, within a control volume (orange dash rectangle) consisting of the solution inside the membrane pore and the boundary layer outside the membrane pore, the mass balance of SDS can be performed considering SDS transports via convection, diffusion, accumulation (in the solution) and adsorption. The distinction between (a) and (b) is the concentration profile of SDS in the control volume (green lines). SDS diffuses into and out of the control volume in (a) and (b), respectively.

For a low SDS concentration in the feed solution, the LEP corresponding to the bulk SDS concentration may be higher than ΔP, which may suggest that pore intrusion should not occur. However, the SDS concentration at the pore entrance (i.e. the feed/membrane interface) can be significantly higher than the bulk concentration due to concentration polarization (CP) [40,41]. If the elevated SDS concentration reaches the critical concentration (c^*), the feed solution is able to enter the membrane pore. Once in the pore, the SDS can adsorb onto the pore surface. The sole effect of adsorption is to reduce the SDS concentration and thus the liquid surface tension at the wetting frontier, not to change the pore surface tension used in LEP calculation. On the other hand, convective transport of SDS tends to increase the SDS concentration at the wetting frontier. These two effects of convective transport and surface adsorption are exactly the same as in the case with high bulk concentration of SDS described in the last paragraph. However, with low bulk concentration of SDS, the direction of diffusion along the pore is opposite to that when the bulk concentration of SDS is high. In another word, diffusion tends to reduce the SDS

concentration at the wetting frontier when the bulk SDS concentration is low. The concentration profile of SDS in the case of low bulk SDS concentration is illustrated in Fig. 1b.

Regardless of the SDS concentration in the feed solution, the transport of SDS within an ideal cylindrical pore can be described by Eq.3 that is derived based on the mass balance of SDS in a control volume including the solution in the boundary layer and the partially wetted membrane pore (Fig. 1):

$$\begin{aligned}\left(J_w c_0 - D\frac{\partial c(x,t)}{\partial x}_{x=0}\right)dx &= \int_0^{\delta_b}[c(x,t+dt)-c(x,t)]dx \\ &+ \varepsilon\left\{\int_{\delta_b}^{\delta_b+l(t+dt)}\left[\frac{2}{R}\tau(x,t+dt)(1-\varepsilon)+c(x,t+dt)\right]dx\right. \\ &\left.- \int_{\delta_b}^{\delta_b+l(t)}\left[\frac{2}{R}\tau(x,t)(1-\varepsilon)+c(x,t)\right]dx\right\}\end{aligned} \tag{3}$$

where J_w is the vapor flux in MD, ε is the porosity of the membrane ($\varepsilon = 0.6$ in our simulation), c_0 is the SDS concentration in bulk solution, t is time, R is the radius of the ideal cylindrical pore, D is the diffusion coefficient of the SDS ($D = 7.3\times10^{-10}$ m^2/s according to literatures[42]), x is the position of a certain point from the starting point of the boundary layer (x=0, see Fig.1) in the direction pointing from the feed solution to the distillate, $c(x,t)$ is the SDS concentration at position "x" and time "t", δ_b is the thickness of the boundary layer (estimated to be 15 μm based on Sherwood correlation and the flow conditions [40,41,43]), $l(t)$ is distance between the pore entrance and the wetting frontier, $\tau(x,t)$ is the surface density of SDS adsorbed on the pore surface at position x, and time t. The left-hand-side of Eq. 3 represents the amount of SDS entering the control volume in the period from time t to $t+dt$, with the first and second terms representing the convective and diffusive components to the flux at the entrance of the membrane pores, respectively. The right-hand-side of Eq.3 represents increase of the total amount of SDS in the control volume within that time period. More detailed explanation of the development of Eq. 3 is given in Appendix A. We note that the control volume as defined is expanding over time as the wetting frontier moves deeper into the pore.

Our ultimate goal of solving Eq.3 is to identify $l(t)$, which quantifies the kinetics of wetting frontier propagation. Solving Eq. 3 requires the relationship between $\tau(x,t)$ and $c(x,t)$ which is described by the adsorption isotherm. The simplest adsorption isotherm is the stepwise adsorption isotherm:

$$\tau(x,t) = \begin{cases}\tau_{max}, & c(x,t) > 0 \\ 0, & c(x,t) = 0\end{cases} \tag{4}$$

where τ_{max} is the maximum surface adsorption density of SDS on polyvinylidene fluoride (PVDF) surface ($\sim 10 \times 10^{-6}$ mole m^{-2} according to literature[44]). The stepwise adsorption isotherm is a valid approximation of Langmuir adsorption isotherm for SDS adsorption onto PVDF membrane surface as justified in Appendix B. With the assumption of stepwise adsorption isotherm, the surface of the wetted pores has τ_{max} everywhere except for the negligibly small differential area at the wetting frontier.

Finding $l(t)$ from Eq.3 also requires the knowledge of $c(x,t)$, which is described by the convection-diffusion equation in the boundary layer (Eq. 5) and by the convection-diffusion-adsorption equation within the pore (Eq. 6):

$$\frac{\partial c(x,t)}{\partial t} = -J_w \frac{\partial c(x,t)}{\partial x} + D \frac{\partial^2 c(x,t)}{\partial x^2} \text{ (for } 0 \le x \le \delta_b) \tag{5}$$

$$\frac{\partial c(x,t)}{\partial t} = -\frac{J_w}{\varepsilon} \frac{\partial c(x,t)}{\partial x} + D \frac{\partial^2 c(x,t)}{\partial x^2} - \frac{2}{R} \frac{\partial \tau}{\partial t} \text{ (for } \delta \le x \le \delta_b + l(t)) \tag{6}$$

The initial condition of these two equations is $c(x,0) = 0$ except for $c(0,0) = c_0$. The two boundary conditions are $c(0,t) = c_0$, and $c(\delta_b + l(t), t) = c^*$, respectively.

The challenge for solving Eqs. 5 and 6 is the moving boundary of the feed solution with in the pore (i.e. $l(t)$ is a function of t). To overcome this problem, we assume a pseudo-steady state for SDS transport at any moment (i.e. $\partial c / \partial \tau \approx 0$). This is a reasonable approximation because the time scale for wetting frontier propagation is significantly larger than the relevant time scale for surfactant transport. With the pseudo-steady assumption, Eqs. 5 and 6 can now be rewritten as:

$$0 = -J_w \frac{dc}{dx} + D \frac{d^2 c}{dx^2} \text{ (for } 0 \le x \le \delta_b) \tag{7}$$

$$0 = -\frac{J_w}{\varepsilon} \frac{dc}{dx} + D \frac{d^2 c}{dx^2} \text{ (for } \delta_b \le x \le \delta_b + l(t)) \tag{8}$$

with the boundary conditions being $c(0) = c_0$, and $c(\delta_b + l(t)) = c^*$, respectively.

We note that Eqs. 7 and 8 are similar to the equations describing the concentration polarization (CP) phenomenon in forward osmosis, FO[45–47]. Specifically, Eq. 7 accounts for CP in the boundary layer, which is the analogous to external concentration polarization (ECP) in FO; whereas Eq. 8 accounts for CP within the membrane pore, which is equivalent to internal concentration polarization (ICP) in FO. Analytical solutions of Eqs. 7 and 8 are available and presented as Eqs. 9 and 10 for the boundary layer and the wetted region within the pore, respectively:

$$c(x) = \frac{(1-\varepsilon)\exp\left(\frac{J_w \delta_b}{D}\right) c_0 + \varepsilon \exp\left[\frac{J_w}{D}\left(\delta_b + \frac{l(t)}{\varepsilon}\right)\right] c_0 - c^*}{(1-\varepsilon)\exp\left(\frac{J_w \delta_b}{D}\right) + \varepsilon \exp\left[\frac{J_w}{D}\left(\delta_b + \frac{l(t)}{\varepsilon}\right)\right] - 1} + \frac{c^* - c_0}{(1-\varepsilon)\exp\left(\frac{J_w \delta_b}{D}\right) + \varepsilon \exp\left[\frac{J_w}{D}\left(\delta_b + \frac{l(t)}{\varepsilon}\right)\right] - 1} \exp\left(\frac{J_w x}{D}\right) \quad (9)$$

$$(\text{for } 0 \le x \le \delta_b)$$

$$c(x) = \frac{c^* \left[(1-\varepsilon)\exp\left(\frac{J_w \delta_b}{D}\right) - 1\right] + \varepsilon c_0 \exp\left[\frac{J_w}{D}\left(\delta_b + \frac{l(t)}{\varepsilon}\right)\right]}{(1-\varepsilon)\exp\left(\frac{J_w \delta_b}{D}\right) + \varepsilon \exp\left[\frac{J_w}{D}\left(\delta_b + \frac{l(t)}{\varepsilon}\right)\right] - 1} + \frac{\varepsilon \exp\left(\frac{J_w \delta_b}{D}\right)(c^* - c_0)}{(1-\varepsilon)\exp\left(\frac{J_w \delta_b}{D}\right) + \varepsilon \exp\left[\frac{J_w}{D}\left(\delta_b + \frac{l(t)}{\varepsilon}\right)\right] - 1} \exp\left(J_w \frac{x - \delta_b}{D\varepsilon}\right) \quad (10)$$

$$(\text{for } \delta_b \le x \le \delta_b + l(t))$$

Given the position of wetting frontier as quantified by $l(t)$, the SDS concentration profile can be obtained using Eqs. 9 and 10. Inserting the spatial distributions of solution concentration of SDS, $c(x)$, at time t and $t + dt$, into Eq.3 allows us to perform a numerical evaluation of the differential time, dt, that is required for the wetting frontier to move forward by a differential distance, dl. Numerical integration of dl from 0 to δ_m, with δ_m being the membrane thickness (180 μm for the membrane tested), yields the time required for the feed solution to fully penetrate a cylindrical pore after the introduction of surfactants into the feed solution. We define this as the wetting breakthrough time, t_{wetting}.

3. Materials and methods

Direct contact membrane distillation (DCMD) experiments were performed to validate the results simulated using the model presented in Section 2. Here, we provide relevant information regarding these experiments.

3.1. Materials and chemicals

The hydrophobic PVDF membrane with a nominal pore size of 0.45 μm and a thickness of 180 μm was procured from GE Healthcare (Pittsburg, PA). Sodium chloride (NaCl), SDS, and Triton X-100 were all purchased from Sigma Aldrich (St. Louis, MO) and used without further purification.

3.2. Surface tension measurements

The surface tensions of aqueous NaCl solutions (0.6 M) containing different concentrations of SDS were measured at 60 °C using drop shape analysis of air bubbles in respective solutions by an optical tensiometer (TL100, Attension Finland). The surface tensions of NaCl solution (0.6 M) with 0.5 mM SDS at different temperatures from 35 to 70 °C were also measured using the same method. For each solution, the reported surface tension is the average of five different measurements.

3.3. Intrinsic contact angle measurements

The direct measurements of contact angle (CA) using PVDF membranes cannot yield relevant information that can be used for calculating LEP based on Eq. 2. This is because the CA in Eq. 2 is the intrinsic CA which can only be measured using a smooth and non-porous surface, as otherwise the system would be in a Cassie-Baxter state and yield a CA that is significantly higher than the intrinsic CA. Therefore, a smooth and non-porous PVDF film was fabricated by first melting the PVDF membrane at 200 °C and then cooling it at room temperature. The roughness of the reconstructed PVDF film was measured by atomic force microscopy (AFM, Dimension ICON, Bruker, Billerica, MA). With the reconstructed PVDF film, the intrinsic CA between the PVDF membrane and the given solutions were measured using captive bubble method. For each SDS concentration, CA measurements were conducted at 5 different positions on the reconstructed PVDF film and the average and standard deviation of the measurements are reported.

3.4. Determination of LEP

With the surface tension of the feed solution and intrinsic CA of the feed solution on the reconstructed PVDF film, we use Eq. 2 to calculate the LEP for each feed solution assuming perfect cylindrical pores (B=1) with a pore radius of $R = 0.225$ μm and $B = 1$. We note that due to fast adsorption of surfactants in membrane pores, LEP cannot be accurately determined using conventional experimental protocol [48,49] because the properties of the wetting frontier differ significantly from those of the bulk solution. We also note that the calculated LEP based on measured parameters and Eq. 2 is merely an estimation due to the simplifying assumption of ideal cylindrical pore.

3.5. DCMD wetting experiments

The membrane wetting experiments were conducted with a standard DCMD experimental setup that was described in detail in our previous studies [50,51]. The feed solution was 0.6 M NaCl aqueous solution with SDS, whereas deionized water was utilized as permeate stream. Both the vapor flux and the conductivity of the permeate stream were continually monitored and recorded with a time interval of 1 minute. The real-time salt rejection of the membrane was calculated using the monitored vapor flux and conductivity data. Without wetting, the salt

rejection of the PVDF membrane is always above 99.9%. In this study, we quantify the kinetic rate of pore wetting by measuring the breakthrough time. t_{wetting}. The breakthrough moment is defined as the point at which a small portion of membrane pores have already been fully penetrated by the feed solution. To be consistent between experiments, we arbitrarily set the time when salt rejection dropped to 99% as the breakthrough moment.

In each experiment, prior to the addition of SDS to induce membrane wetting, the system was operated for half an hour to establish a stable baseline of vapor flux. Three different sets of wetting experiments were performed for the purposes of studying the impacts of three parameters on membrane wetting process. These three parameters include bulk concentration of SDS in feed solution, vapor flux, and transmembrane hydraulic pressure, respectively. In each set of experiments, only the target parameter under investigation was varied, while the other two parameters were maintained constant. The detailed experimental conditions are given in the following discussion section and also summarized in Table A1 in Appendix C.

4. Results and discussions

4.1. The impact of SDS concentration

The model predictions for DCMD membrane wetting with different bulk concentrations of SDS, c_0, are remarkably consistent with the experimental data (Fig. 2). In general, a higher c_0 results in a shorter t_{wetting}. Based on the mass transfer model elaborated in section 2, the kinetics of forward propagation of wetting frontier largely depends on how fast the pore surface is saturated by SDS adsorption, which in turn depends on how fast the SDS molecules are transported from the bulk solution to the wetting frontier. When water flux, J_w, is constant, a higher c_0 enhances both the convective and diffusive transport of SDS to the wetting frontier (when $c_0 < c^*$, a higher c_0 deters the back diffusion), which leads to faster pore wetting as indicated by Fig. 2.

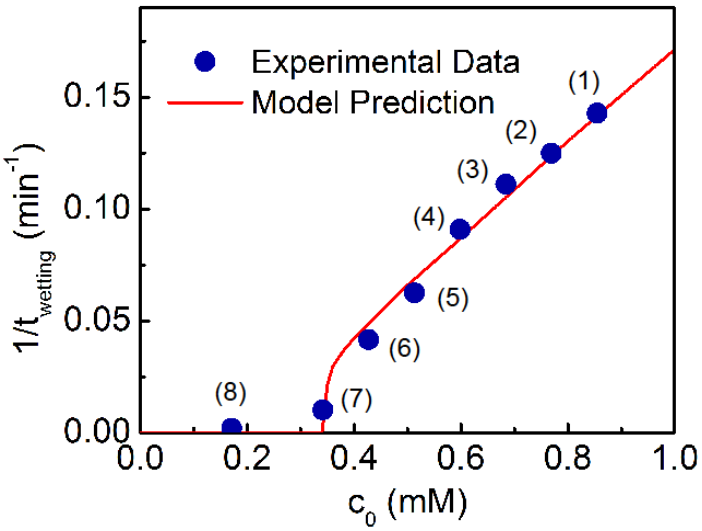

Fig. 2. Experimental results (blue circles) and model prediction (red line) of MD membrane wetting time with different SDS concentrations in feed solution. For the DCMD wetting experiments, different SDS concentrations c_0 ranging from 0.17 to 0.85 mM were evaluated. All other experimental conditions are maintained constant except for c_0. Specifically, the feed and permeate solution temperatures were maintained at 60 and 20 °C, respectively, which resulted in a constant vapor water flux J_w at 32.3 ± 0.9 L $m^{-2} h^{-1}$ prior to the addition of SDS. The transmembrane hydraulic pressure ΔP was maintained at 6 kPa. The time series of water flux and salt rejection for DCMD wetting experiments are given in Fig. A1 in Appendix C. For the simulation, the c_0 and J_w are based the experimental conditions, and the critical SDS concentration c^* in the wetting frontier is assumed to be 0.42 mM which corresponds to an LEP of 6 kPa.

Fig. 2 also suggests that when c_0 was lower than a critical bulk concentration c_0' (~0.35 mM), the membrane was not wetted by the feed solution, which can also be explained by the wetting model. For the feed solution to enter the membrane pore, the SDS concentration at the pore entrance must at least equal the critical SDS concentration c^* (0.42 mM for $\Delta P = 6$ kPa) so that ΔP is higher than LEP calculated using the bulk concentration. If the bulk concentration, c_0, is too low, the concentration at the membrane surface cannot exceed c^* even considering the effect of external concentration polarization (ECP), in which case the feed solution cannot even enter the pores. This critical bulk concentration c_0' below which feed solution cannot enter membrane pore can be determined based on the equation that describes ECP:

$$c_0' = c^* \exp\left(-\frac{J_w \delta_b}{D}\right) \quad (11)$$

4.2. The impact of vapor flux

When flux is increased, convective transport of SDS to the wetting frontier is faster, which in turn accelerates the saturation of the pore surface by SDS and thus the forward propagation of the wetting frontier. Such an effect of vapor flux on wetting kinetics is consistently observed from both experimental data and model simulation (Fig. 3). Specifically, Fig.3 suggests that $1/t_{wetting}$ is a linear function of vapor flux, i.e., the wetting time is roughly inversely proportional to the vapor flux. We note that the surface tension of the feed solution did not change much with temperature varying from 35 to 70 °C indicated by all of the measured values fell in the range of 32.4 ±3.5 mN/m.

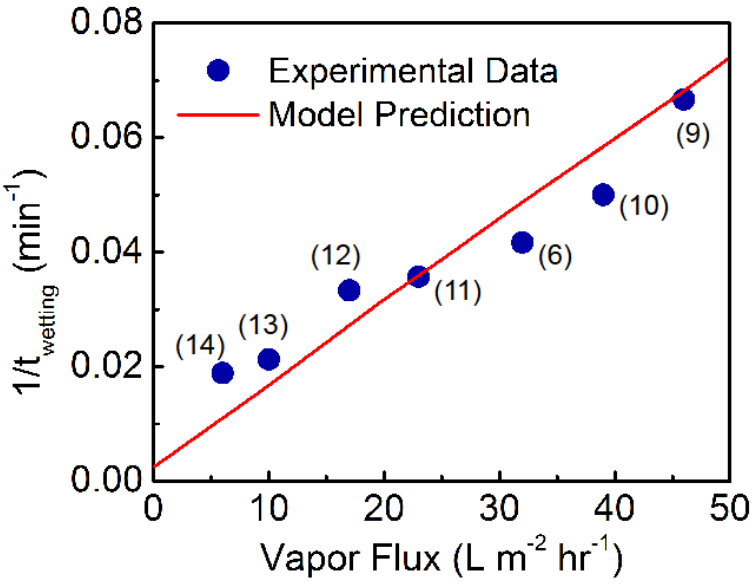

Fig. 3. Experimental results (blue circles) and model prediction (red line) of MD membrane wetting at different vapor fluxes. In the DCMD wetting experiments, the permeate solution temperature was maintained at 20 °C, whereas the feed solution temperatures varied from 35 to 70 °C, which resulted in varied vapor water flux J_w from 6.0 to 45.8 L m^{-2} h^{-1}. Except for the feed solution temperature, all experimental conditions are maintained the same. Specifically, the SDS concentration c_0 of the feed solution was 0.43 mM, and the transmembrane hydraulic pressure ΔP was 6 kPa. The detailed water flux and salt rejection rate data for DCMD wetting experiments were shown in Fig. A2 in Appendix D. For model simulation, c_0 and J_w are based on the experimental conditions, and the critical SDS concentration c^* in the wetting frontier is assumed to be 0.42 mM which corresponds to an LEP of 6 kPa.

We also observe that the simulated the "$1/t_{wetting}$ vs. flux" line does not pass the origin, which suggests that wetting can still occur with zero vapor flux, although it takes a very long breakthrough time. Wetting can occur in the absence of vapor flux due to transport of SDS to the wetting frontier via diffusion, if the bulk surfactant concentration is sufficiently high. However, in the case described by Fig.3, we can conclude that vapor flux induced convective transport has a dominant effect on the overall SDS transport as long as the flux is not too low.

4.3. The impact of transmembrane hydraulic pressure

In addition to the influences of surfactant concentration and vapor flux, the impact of transmembrane hydraulic pressure, ΔP, was also investigated. As described in section 2, the system is considered to be always in a force equilibrium described by the continuous equality between ΔP and LEP. Because LEP is a function of $\gamma_L \cos\theta$ (we do not separate γ_L and $\cos\theta$, because θ is dependent on γ_L, anyway.) which is in turn a function of surfactant concentration, each ΔP corresponds to a critical surfactant concentration, c^*, at the wetting frontier. With the force equilibrium condition ($LEP = \Delta P$), the impact of ΔP is eventually exerted via the

corresponding c^* that serves as the boundary condition for solving the pseudo-steady state surfactant transport equation (Eq. 8).

We note that for a given ΔP, c^* is dependent on the surfactant species, salt composition, and surface tension of the pore surface, which all have significant influence on $\gamma_L \cos\theta$ (as a function of surfactant concentration), and on pore geometry, which also has a strong impact on LEP. However, the dependence of c^* on temperature is weak due to the weak dependence of γ_L on temperature. Due to the complex relation between c^* and ΔP the establishment of which requires the knowledge of other parameters and relation (e.g. $\gamma_L \cos\theta$ as a function of surfactant concentration), in the following analysis, we will use c^* as a proxy variable of ΔP when we systematically study the impact of ΔP on the wetting kinetics. For a given system with known surfactant species, salt composition, material and morphological properties of the membrane, there exists a one-to-one relation between ΔP and its proxy variable c^*. Although not particularly straightforward, this treatment using c^* as a proxy variable allows us to focus on the wetting mechanism itself without having to arbitrate several unknown parameters and relations. In the following analysis, all simulation will be carried out using c^* as the variable to generate the wetting time. In the few experimental measurements, however, we will estimate the c^* based on ΔP and other estimated properties and relations.

Fig. 4 shows the simulation results of $1/t_{wetting}$ as a function of c^* with different c_0 at the same vapor flux. The relative positions of the different $1/t_{wetting}$ vs. c^* curves with different c_0 suggest that increasing the bulk concentration of SDS in the feed solution accelerates the wetting process, which is consistent with the results in Fig. 2. Within each curve, increasing c^*, which is equivalent to decreasing ΔP, slows down pore wetting. While ΔP itself does not have direct impact on SDS transport, a lower ΔP leads to a higher c^* based on the force equilibrium assumption. Regardless of c_0, a higher c^* always contributes negatively to the transport of SDS to the wetting frontier. In particular, when c^* is sufficiently high, the forward convection is offset by the back diffusion, resulting in no net transport of SDS to the wetting frontier. This maximum c^*, c^*_{max}, beyond which wetting does not occur is given by

$$c^*_{max} = c_0 \exp\left(\frac{J_w \delta_b}{D}\right) \quad (12)$$

This c^*_{max} correspond to a critical ΔP below which wetting would not occur. Such ΔP is essentially the LEP calculated using Eq.2 with the $\gamma_L \cos\theta$ the surfactant concentration of the c^*_{max}. We note that LEP can even become negative when the surfactant concentration is sufficiently high, in which the force equilibrium condition requires that distillate hydraulic pressure be higher than the feed hydraulic pressure.

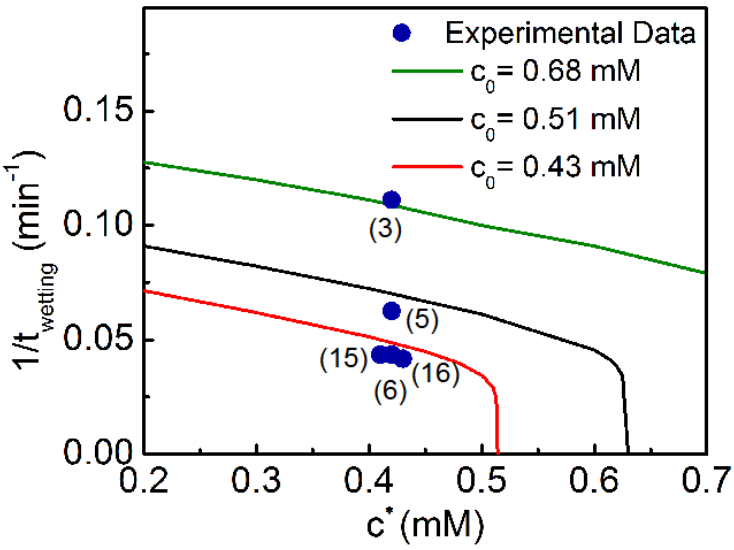

Fig. 4. Experimental results (blue circles) and model predictions (red line for c_0 = 0.43 mM, black line for c_0 = 0.51 mM, and green line for c_0 = 0.68 mM) of DCMD membrane wetting experiments with different critical concentrations c^* that depends on the transmembrane hydraulic pressure ΔP and is thus employed to serve as a proxy variable to ΔP without the detailed knowledge of solution and membrane properties. For DCMD wetting experiments with c_0 = 0.43 mM, three different ΔP were employed (0, 6, and 12 kPa), and the critical concentrations c^* were estimated by LEP calculation results in Appendix I. For DCMD wetting experiments with c_0 = 0.51 and 0.68 mM, ΔP was controlled to be 6 kPa. In all wetting experiments, the feed and permeate solution temperatures were maintained at 60 and 20 °C, respectively, which resulted in a constant vapor water flux J_w at 32.1 ± 0.8 L $m^{-2} h^{-1}$ prior to the addition of SDS. The detailed water flux and salt rejection rate data for DCMD wetting experiments were shown in Fig. A3 in Appendix E. For the model simulations, three different c_0 (0.43, 0.51, 0.68 mM) were investigated with the same J_w at 32 L $m^{-2} h^{-1}$, respectively. For the experimental results, with c_0 = 0.43 mM, $t_{wetting}$ is 25, 24, and 24 min for ΔP = 0, 6, and 13 kPa, respectively; with c_0 = 0.51 mM, $t_{wetting}$ = 17 min for ΔP = 6 kPa; with c_0 = 0.68 mM, $t_{wetting}$ = 9 min for ΔP = 6 kPa.

To compare the model prediction with the experimental data from MD wetting experiments using different ΔP, the quantitative relationship between ΔP and c^* is required. However, accurate measurement of LEP using conventional approach is not applicable for solution with surfactants due to the rapid adsorption of surfactants onto the pore surface which leads to a significant difference of surfactant concentration between the bulk solution and the wetting frontier. Therefore, we have estimated the LEP using Eq. 2 with measured surface tension and the intrinsic CA of the solution on a smooth, reconstructed PVDF surface. (detailed results are shown in Fig. A4, A5 and A6). The intrinsic CA cannot be measured using the PVDF membrane due to the presence of the pores, as a sessile drop on a porous PVDF membrane surface is in a Cassie-Baxter state that yields a CA significantly higher than the intrinsic CA [52,53].

As shown in Fig. 4, LEP decreases with the increasing c^*. It can be observed from Fig. A3 and A7 (Appendix F and J) that the range of ΔP investigated in our experiments only corresponds to very small change in c^*. Using linear interpolation, we estimate the c^* corresponding to the tested ΔP of 0, 6, and 12 kPa to be 0.43, 0.42, and 0.41 mM, respectively. Within such a small range of c^*, the kinetic model predicts that breakthrough time should be very similar, which is indeed observed from experiments. While the range of c^* of the three investigated cases seems small, the corresponding range of ΔP is actually significant in the context of MD, because (1) MD is not a pressurized membrane process and only requires relatively small hydraulic pressures to circulate the feed and distillate streams, and more importantly, (2) ΔP represents the transmembrane hydraulic pressure which is typically zero when the feed and distillate stream have the same hydraulic pressures. Therefore, the experimental data was not collected to validate a full simulated curve on Fig. 4 because ΔP for the lower range of c^* is too high in the context of MD and is thus practically irrelevant.

The "clustering" of the three data points for ΔP=0, 6, and 12 kPa (when c_0 = 0.43 mM) suggests that wetting kinetics in MD is virtually independent of ΔP, which is quite counter-intuitive because the very criterion of wetting is ΔP > LEP. The key to resolve this counter-intuition is to understand the pseudo steady-state and force equilibrium assumption in the wetting model, that, ΔP does not exert its impact directly by inducing force unbalance, but rather by affecting the SDS concentration at the wetting frontier required to maintain the force balance, which in turn impacts the mass transfer rate of SDS to the wetting frontier.

4.4. Interplay of multiple factors in membrane wetting kinetics

Now that kinetic model of wetting has been validated experimentally by varying individual operational parameter including SDS concentration, vapor flux, and transmembrane pressure, such a model can be employed to systematically investigate the combined effect of different parameters. We simulate the "$1/t_{wetting}$ vs. c_0" curves by varying J_w, c^* (as a proxy of ΔP), and the type of surfactants. In all cases, the simulated curves show the characteristic shape observed in Fig. 2. Specifically, wetting does not occur (i.e. $1/t_{wetting}$=0) until c_0 reaches a certain critical concentration, c_0'. Beyond such critical concentration, $1/t_{wetting}$ eventually becomes linear to c_0.

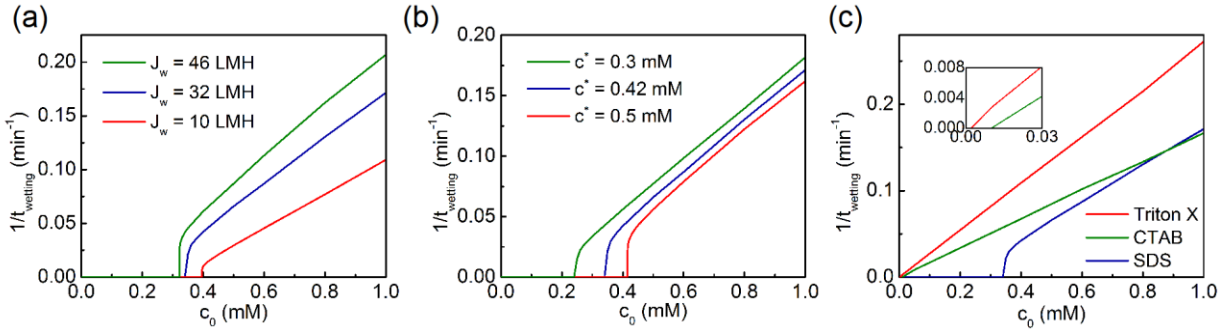

Fig. 5. (a) Simulations of $1/t_{wetting}$ as a function of c_0 in MD wetting with different SDS concentrations c_0 and vapor fluxes J_w (green line for J_w = 46 L m^{-2} h^{-1} blue line for J_w = 32 L m^{-2} h^{-1},and red line for J_w = 10 L m^{-2} h^{-1}). In the predictions, the critical SDS concentration c^* in the wetting frontier is 0.42 mM.

(b) Modeling predictions of DCMD membrane wetting with different c_0 and c^* (green line for $c^* = 0.5$ mM, blue line for $c^* = 0.42$ mM, and red line for $c^* = 0.3$ mM). In the preditions, J_w is fixed at 32 L m^{-2} h^{-1}. (c) Modeling predictions of DCMD membrane wetting with different c_0 of different surfactant species (red line for Triton X-100, green line for cetrimonium bromide (CTAB), and blue line for SDS). The inset is the zoom-out view of the model predictions of Triton X-100 and CTAB with very small c_0. In the predictions, J_w is constant at 32 L m^{-2} h^{-1}. For different species, both the maximum surface adsorption density τ_{max} and c^* are different. The τ_{max}, c^* and D for Triton X-100 are 3.1×10^{-6} mole m^{-2}, 0.04 mM and 4×10^{-11} m^2 s^{-1}, respectively[54,55]. The τ_{max}, c^* and D for CTAB are 5×10^{-6} mole m^{-2}, 0.02 mM and 3.9×10^{-11} m^2 s^{-1}, respectively[56,57].

With SDS surfactant and a fixed ΔP (equivalent to c^*=0.42 mM), wetting in general occurs faster (i.e. $1/t_{wetting}$ increases) with a higher J_w across the full range of c_0 (Fig. 5(a)), which is consistent with the discussion in section 4.2. Interestingly, the critical concentration, c_0', decreases with increasing J_w, which suggests that pore wetting becomes easier in an operation with a high vapor flux. This can be explained by the ECP effect as described by Eq. 11. The stronger effect of ECP as a result of a higher J_w reduces the bulk concentration required to achieve c^* at the pore entrance, which is necessary for pore wetting to start.

On the other hand, increasing c^*shifts the "$1/t_{wetting}$ vs. c_0" curve toward the right (Fig 5(b)), which suggests that reducing ΔP actually deters pore wetting. This dependence of wetting kinetics on ΔP has been explained in detail in section 4.3. Although c^* is introduced as a proxy variable for ΔP given all other parameters maintained constant, it can also be employed to capture the impacts of other parameters. For example, increasing the salt concentration of the feed solution will reduce the surface tension for a given surfactant concentration, and thereby reduces the c^* for a given ΔP. Therefore, we can conclude that increasing the salt concentration without changing other parameters will accelerate pore wetting. Similarly, if the surface tension of the membrane material increases, the intrinsic CA of a given solution will increase. Consequently, the c^* needed to reach a certain LEP (=ΔP) according to Eq.2 increases, which will slow down pore wetting.

For membrane wetting with different surfactants including nonionic surfactant Triton X-100, cationic surfactant CTAB, and ionic surfactant SDS, the dynamic wetting behaviors are qualitatively similar but quantitatively very different (Fig. 5(c)). There are three major attributes of a surfactant that influence the kinetics of wetting based on our model. These three attributes include (1) the effectiveness of surfactant in modifying the surface tension of the feed solution and the intrinsic CA, which affects the c^* for a given ΔP, (2) the diffusion coefficient, which affects the mass transfer of surfactants to the wetting frontier, (3) the maximum packing density of surfactants, τ_{max}, which affects how fast the pore surface is saturated by adsorbed surfactants.

Due to the combined effect of these three contributions, the simulated "$1/t_{wetting}$ vs. c_0" curves for the three surfactants are very different in two aspects: (a) the critical bulk concentration of surfactants, c_0', below which wetting does not occur, and (b) the slope of the "$1/t_{wetting}$ vs. c_0" curve when c_0 is higher than c_0', which represents the effectiveness of

increasing c_0 beyond the critical concentration in accelerating pore wetting. The first aspect (a) is primarily determined by attribute (1), i.e., the effectiveness of surfactant in modifying the surface tension of the feed solution and the intrinsic CA. To reduce $\gamma_L \cos\theta$ to any given level from that of surfactant-free feed water, the surfactant (molar) concentration required for SDS is significantly higher than that for CTAB and Triton X-100. Therefore, the critical bulk concentration c_0' for SDS is also significantly higher than that for CTAB and Triton X-100.

The second aspect (b) is intricately dependent on both diffusion coefficient, D, and maximum surface packing density, τ_{max}. Such an intricate dependence can only be revealed by numerically solving the full kinetic model established in section 2. In general, a large diffusion coefficient and a small τ_{max} both promote faster pore wetting, leading to more sensitive response of $t_{wetting}$ to the increase of bulk concentration c_0. The diffusion coefficients and maximum surface packing density of the three surfactants are summarized in Table 1. Fig. 5(c) suggests that increasing c_0 beyond c_0' has approximately equal effectiveness in accelerating pore wetting induced by SDS and Triton X-100 (i.e. the slopes are roughly the same in both cases), even though the two surfactants have large differences in D and τ_{max} as shown in Table 1. On the other hand, CTAB has as similar D as Triton X-100, but its τ_{max} is ~60% higher. Consequently, increasing c_0 for CTAB is not as effective in accelerating pore wetting as increasing c_0 for Triton X-100, as represented by a smaller slope for CTAB.

Table 1. Diffusion coefficient and maximum surface packing density for different surfactants

	SDS	CTAB	Triton X-100
Diffusion coefficient, D ($\times 10^{-11}$ m^2 s^{-1})	73	3.9	4.0
Maximum surface packing density, τ_{max} ($\times 10^{-6}$ mole m^{-2})	10	5	3.1

5. Conclusion

In this study, we developed and numerically solved a kinetic model for dynamic pore wetting induced by surfactants in MD. This kinetic transport model is developed by solving the coupled convection-diffusion-adsorption mass transport equations using assumptions of pseudo-equilibrium adsorption and force equilibrium at the wetting frontier, as well as pseudo-steady state for surfactant transport in the boundary layer and within the partially wetted pore. The kinetic model suggests several characteristic dependences of wetting kinetics on bulk surfactant concentration, vapor flux, and transmembrane hydraulic pressure, which have been validated by MD experiments with pore wetting induced by addition of SDS surfactant. We believe the developed model is universally applicable for predicting kinetics of pore wetting induced by other surfactants or any highly surface-active agents that can (1) significantly change the surface

tension of an aqueous solution even at low concentration, and (2) strongly adsorb onto the pore surface.

The proposed and validated model reveals several important insights regarding surfactant-induced pore wetting, which are summarized below:

(1) Surfactants promote wetting by reducing the surface tension of the feed solution, not by making the pore surface hydrophilic.
(2) For the above reason, adsorption of surfactants onto the pore surface does not promote wetting. On the contrary, it deters pore wetting by continuously removing the surfactant at the wetting frontier and thereby increasing its LEP.
(3) The kinetics of surfactant-induced pore wetting is determined dominantly by the transport of surfactants to the wetting frontier, which is governed by convection, diffusion, and surface adsorption.

These insights will help us better understand pore wetting in MD and develop effective strategies to mitigate pore wetting in MD operations.

Acknowledgements

This work is supported by National Science Foundation via research grant CBET-1739884. Z. Wang also acknowledge the support from American Chemical Society Petroleum Research Foundation via award ACS-PRF 57353 DNI.

Appendix A. Derivation of mass balance equation for surfactants (Eq. 3).

Eq.3 with a slight modification is shown below and denoted as Eq.3'. Eq.3 in the main text can be obtained by dividing both sides of Eq.3' by πR^2. Eq. 3 or Eq. 3' describes the mass balance of surfactants in the control volume (CV, including boundary layer and pores). The definition of each term can be found in the main text and the nomenclature. Here, we provide a more detailed description of the meaning of each term.

$$\begin{aligned}\frac{\pi R^2}{\varepsilon}\left(J_w c_0 - D\frac{\partial c(x,t)}{\partial x}_{x=0}\right)dt \\ = \frac{\pi R^2}{\varepsilon}\int_0^{\delta_b}[c(x,t+dt)-c(x,t)]dx \\ + \left\{\int_{\delta_b}^{\delta_b+l(t+dt)}[\tau(x,t+dt)2\pi R(1-\varepsilon)+c(x,t+dt)\pi R^2]dx\right. \\ \left. - \int_{\delta_b}^{\delta_b+l(t)}[\tau(x,t)2\pi R(1-\varepsilon)+c(x,t)\pi R^2]dx\right\}\end{aligned} \quad (3')$$

Here we consider a cylindrical pore of radius R and its corresponding portion in the boundary layer. Because the boundary layer has no solid material and is 100% porous, the area of the boundary layer corresponding to a pore of an area πR^2 is $\pi R^2/\varepsilon$. The first term on the left-hand-side (LHS), $J_w c_0 \pi R^2/\varepsilon$, is the convective flux of the surfactants into the CV corresponding to a pore (including the boundary layer outside the pore). The second term on the LHS is the diffusive flux of surfactants into the same CV. The first integral on the right-hand-side (RHS) represents the accumulation of surfactants in the boundary layer from t to $t+dt$.

The first part of the second integral on the RHS, $\int_{\delta_b}^{\delta_b+l(t+dt)}\tau(x,t+dt)2\pi R(1-\varepsilon)dx$, quantifies the amount of surfactant on the pore surface at time $t+dt$. The term $(1-\varepsilon)$ accounts for the fact that a pore does not have continuous, non-porous wall across the thickness of the membrane. Rather, we assume the isotropy for the membrane porosity so that the available area of solid surface in the pore is $(1-\varepsilon)$ of the area calculated using a cylindrical tube (i.e. $\pi R^2 l(t+dt)$). The second part of the second integral on the RHS is the amount of surfactant in the solution within the pore. The third integral on the RHS is almost exactly the same as the second integral on the RHS except for a different time point, $t+dt$ (instead of t). Together, the difference between the second and the third integrals on the RHS represents the accumulation of surfactants within a pore (not including the boundary layer). The RHS quantifies the accumulation of surfactants within a CV including both the pore and the boundary layer.

Appendix B. Surfactant adsorption isotherm.

Assuming Langmuir adsorption isotherm for SDS adsorption onto PVDF surface [44,58], the area density of the adsorbed SDS on PVDF surface, τ, can be expressed as

$$\tau = \tau_{max} \frac{Kc}{1 + Kc} \quad \text{(A1)}$$

where τ_{max} is the maximum area density of SDS on PVDF surface and K is an equilibrium constant that governs the partition of SDS between the pore surface and the solution phase. According to literatures [44], K can be approximated as 180 mM^{-1}. In our study, the minimum c_0 we utilized was over 0.1 mM. According eq. A1, with $K = 180\ mM^{-1}$ and $c = 0.1\ mM$, $\tau = 0.95\tau_{max}$. With all other concentrations tested, the pore surface can be considered to be practically saturated with SDS as long as the it is in contact with the solution, in which case we can simplify the Langmuir adsorption isotherm to a stepwise adsorption isotherm:

$$\tau = \begin{cases} \tau_{max}, c > 0 \\ 0, c = 0 \end{cases} \quad \text{(A2)}$$

Appendix C. Summary of experimental conditions of DCMD wetting experiments

Table S1. Summary of experimental conditions of DCMD wetting experiments

Experiment No.	SDS concentration (mM)	Feed temperature (°C)	Permeate temperature (°C)	Feed velocity (m/s)	Permeate velocity (m/s)
(1)	0.85	60	20	0.29	0.18
(2)	0.77	60	20	0.29	0.18
(3)	0.68	60	20	0.29	0.18
(4)	0.60	60	20	0.29	0.18
(5)	0.51	60	20	0.29	0.18
(6)	0.43	60	20	0.29	0.18
(7)	0.34	60	20	0.29	0.18
(8)	0.17	60	20	0.29	0.18
(9)	0.43	70	20	0.29	0.18
(10)	0.43	65	20	0.29	0.18
(11)	0.43	55	20	0.29	0.18
(12)	0.43	50	20	0.29	0.18
(13)	0.43	40	20	0.29	0.18
(14)	0.43	35	20	0.29	0.18
(15)	0.43	62	20	0.18	0.18
(16)	0.43	62	20	0.29	0.02

Appendix D. Water fluxes and salt rejection rates data for Fig. 2.

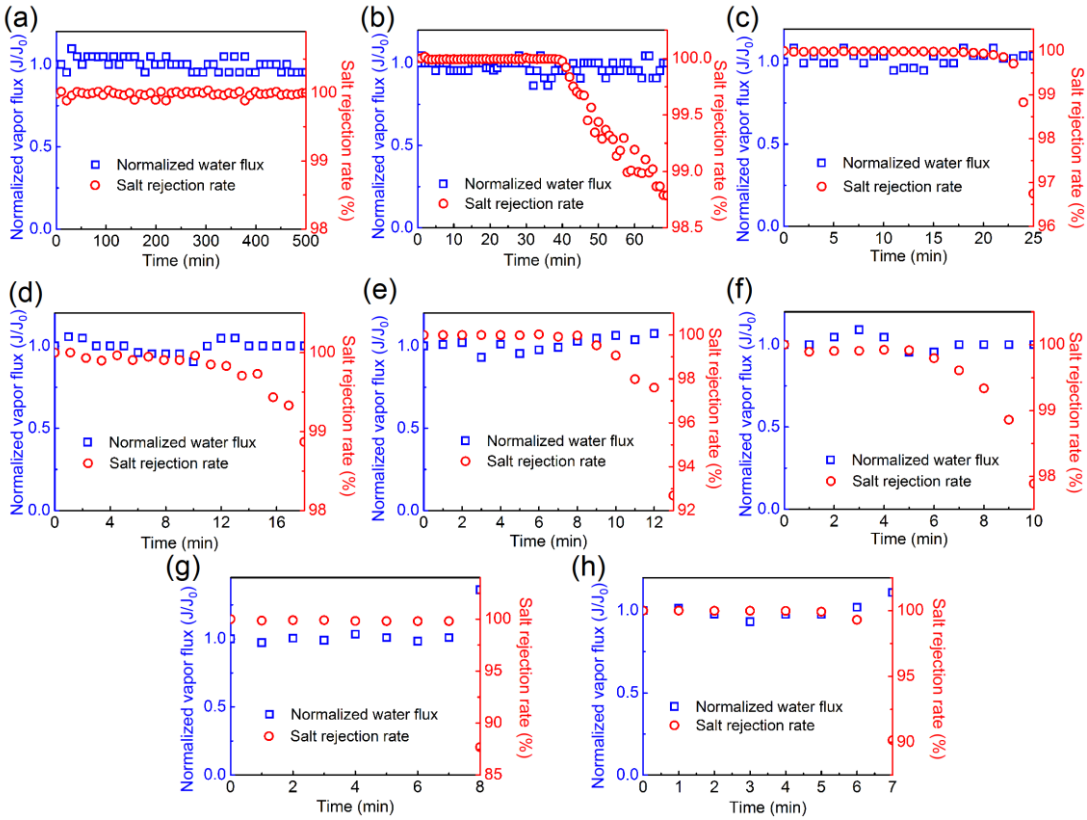

Fig. A1. Normalized water fluxes and salt rejection data for DCMD membrane wetting experiments (experiments 1-9 in Appendix C). In each panel, the water vapor fluxes were normalized by the initial vapor flux. The initial water vapor fluxes were (a) 31.2, (b) 32.7, (c) 32.2, (d) 31.2, (e) 31.4, (f) 32.7, (g) 31.8, and (h) 33.5 L m^{-2} h^{-1}, respectively. The transmembrane hydraulic pressure in all the experiments was 6 kPa. We note that after the membrane was wetted, the normalized water flux increased over unity. This is because the higher hydraulic pressure of the feed stream (than that of the distillate stream) drives convective flow of feed solution through the wetted pores, thereby increasing the total flux.

Appendix E. Water fluxes and salt rejection rates data for Fig. 3.

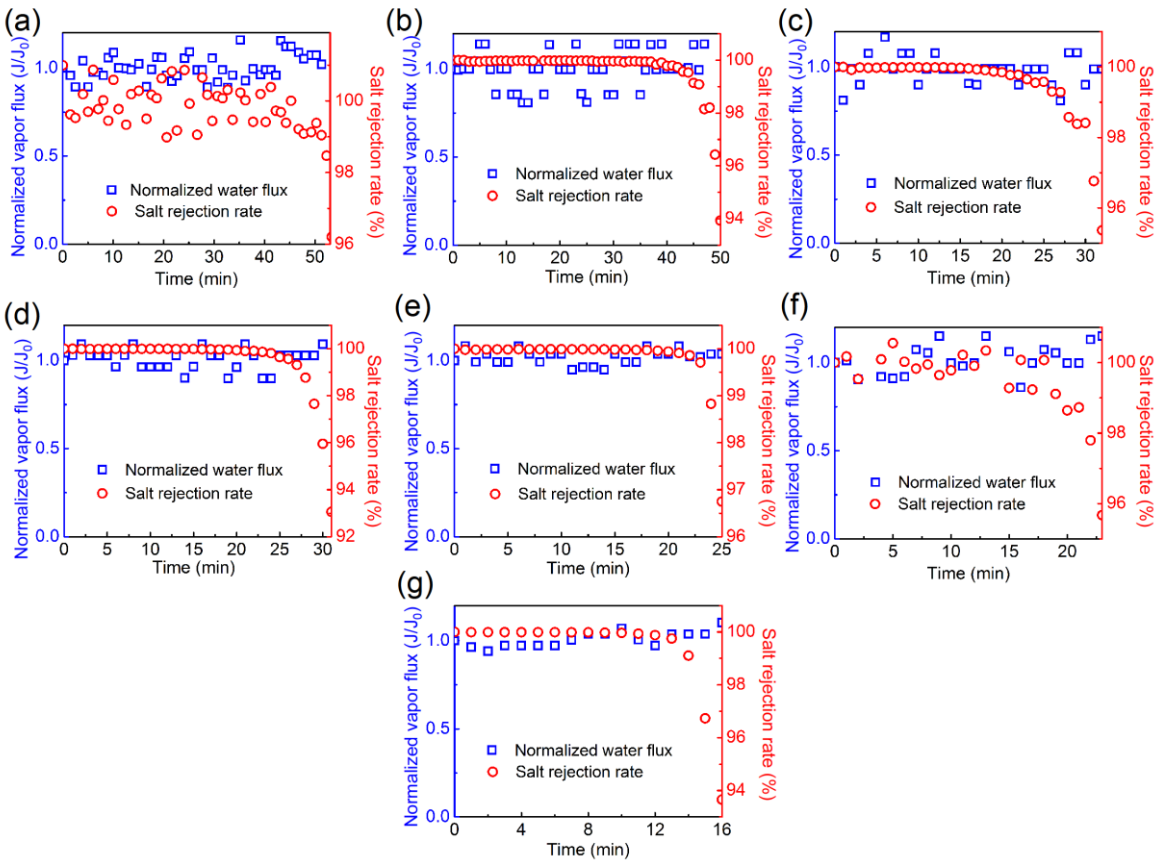

Fig. A2. Normalized water fluxes and salt rejection rates data for DCMD membrane wetting experiments (experiments 6 and 10-14 in Appendix C) with initial vapor fluxes of (a) 6.0, (b) 10.3, (c) 16.5, (d) 23.1, (e) 32.2, (f) 39.2, and (g) 45.8 L m^{-2} h^{-1}, respectively. In each panel, the water fluxes were normalized by the initial vapor flux. The SDS concentration of 0.43 mM and the transmembrane hydraulic pressure of 6 kPa were used in all the experiments. The normalized water flux increased over unity after wetting occurred, as explained in the caption Fig. A1.

Appendix F. Water fluxes and salt rejection rates data for Fig. 4.

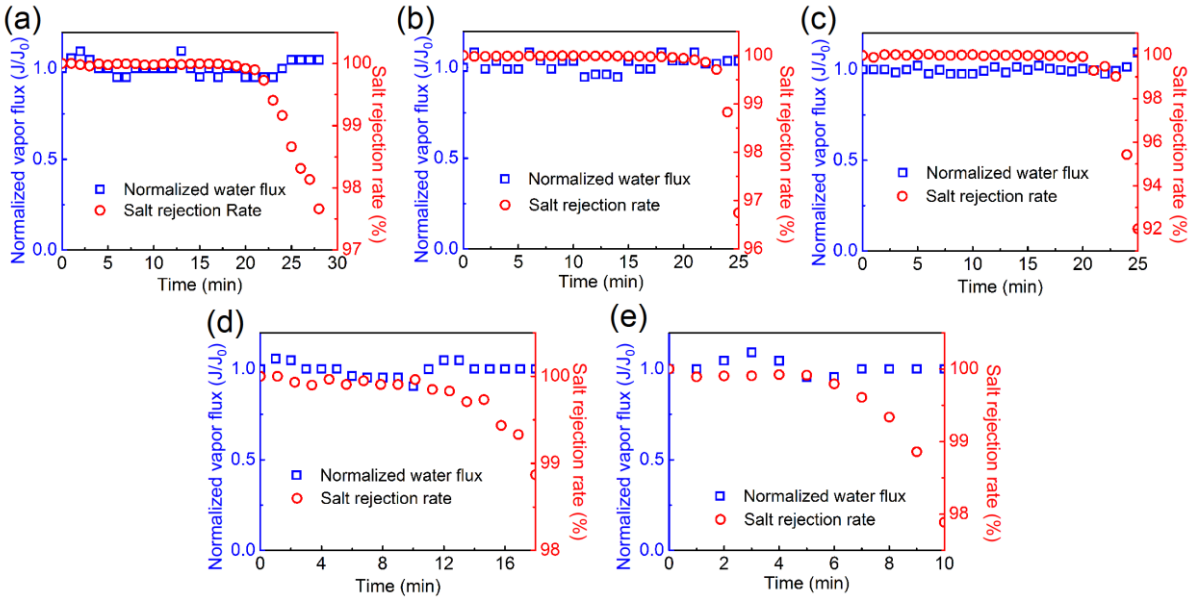

Fig. A3. Normalized water fluxes and salt rejection rates data for DCMD membrane wetting experiments (experiments 6, 15 and 16 in Appendix C) with SDS concentration of 0.43 mM and transmembrane hydraulic pressure of (a) 0 kPa, (b) 6 kPa, and (c) 13 kPa, respectively. Normalized water fluxes and salt rejection rates data for DCMD membrane wetting experiments (experiments 5 and 3 in Appendix C) with transmembrane hydraulic pressure of 6 kPa and SDS concentration of (d) 0.51 mM and (e) 0.68 mM, respectively. In each panel, the water fluxes were normalized by the initial vapor flux. The initial vapor fluxes were (a) 31.2, (b) 32.2, (c) 33.5, (d) 31.2 and (e) 32.7 L m^{-2} h^{-1}, respectively. The normalized water flux increased over unity after wetting occurred, as explained in the caption Fig. A1..

Appendix G. Surface roughness of the reconstructed PVDF film

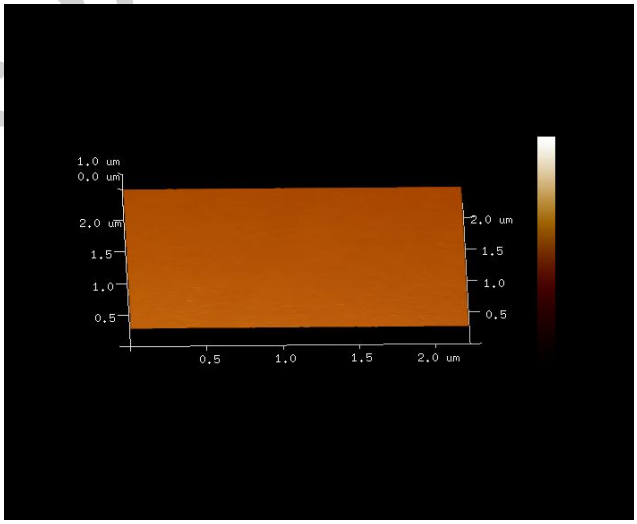

Fig. A4. AFM images of the PVDF film reconstructed from porous PVDF membrane. The measured Ra and Rq were 2.5 and 3.12 nm, respectively. No pore was observed and the

roughness is negligibly small. Therefore, CA measured using this film can be considered as a approximation of the intrinsic CA.

Appendix H. Surface tensions of SDS solutions with different concentrations

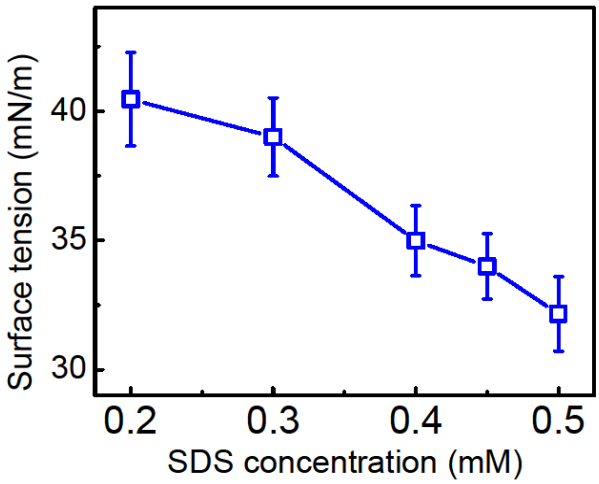

Fig. A5. Surface tensions of NaCl solutions (0.6 M) with different concentrations of SDS.

Appendix I. Intrinsic contact angles of NaCl solutions with different concentrations of SDS on a PVDF surface;

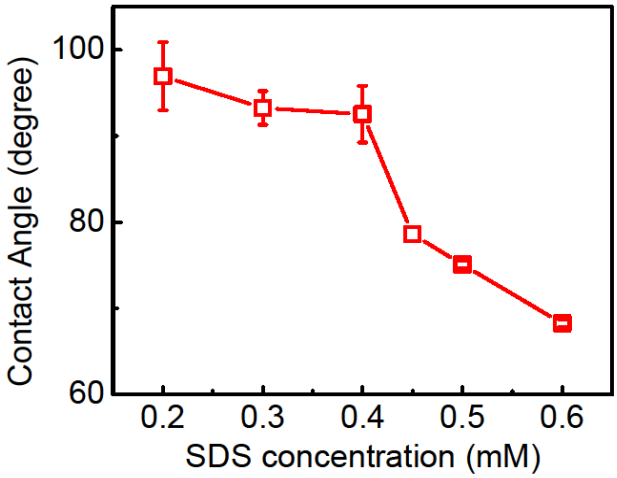

Fig. A6. Intrinsic contact angles of NaCl solutions (0.6 M) with different concentrations of SDS on PVDF surface.

Appendix J. Estimated LEP for NaCl solutions with different SDS concentrations

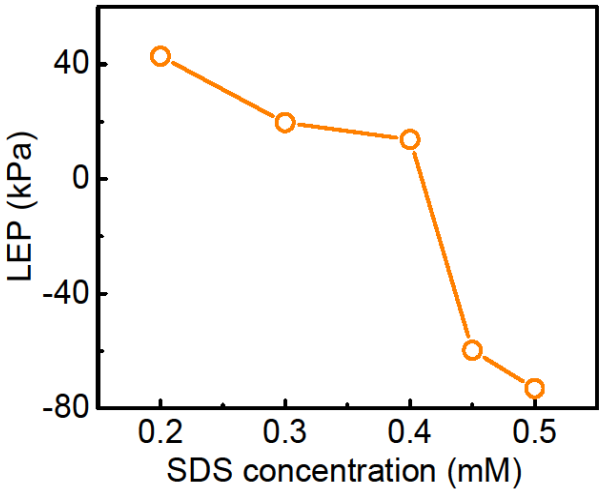

Fig. A7. Estimated LEP of the PVDF membrane for NaCl solutions with different SDS concentrations. These values were calculated using Eq. 2 based on the surface tensions (Fig. A5) and intrinsic contact angles (Fig. A6) of NaCl solutions with different SDS concentrations.

References

[1] K.W. Lawson, D.R. Lloyd, Membrane distillation, J. Memb. Sci. 124 (1997) 1–25. doi:10.1016/S0376-7388(96)00236-0.

[2] M. Khayet, T. Matsuura, Membrane Distillation, first ed., Elsevier, Amsterdam, 2011. doi:10.1016/B978-0-444-53126-1.10016-8.

[3] A. Alkhudhiri, N. Darwish, N. Hilal, Membrane distillation: A comprehensive review, Desalination. 287 (2012) 2–18. doi:10.1016/j.desal.2011.08.027.

[4] F. Banat, N. Jwaied, Economic evaluation of desalination by small-scale autonomous solar-powered membrane distillation units, Desalination. 220 (2008) 566–573. doi:10.1016/j.desal.2007.01.057.

[5] S. Al-Obaidani, E. Curcio, F. Macedonio, G. Di Profio, H. Al-Hinai, E. Drioli, Potential of membrane distillation in seawater desalination: Thermal efficiency, sensitivity study and cost estimation, J. Memb. Sci. 323 (2008) 85–98. doi:10.1016/j.memsci.2008.06.006.

[6] Y.D. Kim, K. Thu, N. Ghaffour, K. Choon Ng, Performance investigation of a solar-assisted direct contact membrane distillation system, J. Memb. Sci. 427 (2013) 345–364. doi:10.1016/j.memsci.2012.10.008.

[7] J. Bundschuh, N. Ghaffour, H. Mahmoudi, M. Goosen, S. Mushtaq, J. Hoinkis, Low-cost low-enthalpy geothermal heat for freshwater production: Innovative applications using thermal desalination processes, Renew. Sustain. Energy Rev. 43 (2015) 196–206. doi:10.1016/j.rser.2014.10.102.

[8] N. Ghaffour, J. Bundschuh, H. Mahmoudi, M.F.A. Goosen, Renewable energy-driven desalination technologies: A comprehensive review on challenges and potential applications of integrated systems, Desalination. 356 (2014) 94–114. doi:10.1016/j.desal.2014.10.024.

[9] D.L. Shaffer, L.H. Arias Chavez, M. Ben-Sasson, S. Romero-Vargas Castrillón, N.Y. Yip, M. Elimelech, Desalination and reuse of high-salinity shale gas produced water: drivers, technologies, and future directions., Environ. Sci. Technol. 47 (2013) 9569–83. doi:10.1021/es401966e.

[10] C.R. Martinetti, A.E. Childress, T.Y. Cath, High recovery of concentrated RO brines using forward osmosis and membrane distillation, J. Memb. Sci. 331 (2009) 31–39. doi:10.1016/j.memsci.2009.01.003.

[11] T. Tong, M. Elimelech, The Global Rise of Zero Liquid Discharge for Wastewater Management: Drivers, Technologies, and Future Directions, Environ. Sci. Technol. 50 (2016) 6846–6855. doi:10.1021/acs.est.6b01000.

[12] P.D. Dongare, A. Alabastri, S. Pedersen, K.R. Zodrow, N.J. Hogan, O. Neumann, et al., Nanophotonics-enabled solar membrane distillation for off-grid water purification, Proc. Natl. Acad. Sci. 114 (2017) 6936–6941. doi:10.1073/pnas.1701835114.

[13] J. Wu, K.R. Zodrow, P.B. Szemraj, Q. Li, Photothermal Nanocomposite Membranes for Direct Solar Membrane Distillation, J. Mater. Chem. A. 5 (2017) 23712-23719. doi:10.1039/C7TA04555G.

[14] M.R. Qtaishat, T. Matsuura, Modelling of pore wetting in membrane distillation compared with pervaporation, in: Pervaporation, Vap. Permeat. Membr. Distill. Princ. Appl., 2015: pp. 385–413. doi:10.1016/B978-1-78242-246-4.00013-1.

[15] E. Guillen-Burrieza, M.O. Mavukkandy, M.R. Bilad, H.A. Arafat, Understanding wetting phenomena in membrane distillation and how operational parameters can affect it, J. Memb. Sci. 515 (2016) 163–174. doi:10.1016/j.memsci.2016.05.051.

[16] Y. Liao, R. Wang, A.G. Fane, Engineering superhydrophobic surface on poly(vinylidene fluoride) nanofiber membranes for direct contact membrane distillation, J. Memb. Sci. 440 (2013) 77–87. doi:10.1016/j.memsci.2013.04.006.

[17] Z. Wang, S. Lin, Membrane fouling and wetting in membrane distillation and their mitigation by novel membranes with special wettability, Water Res. 112 (2017) 38–47. doi:http://dx.doi.org/10.1016/j.watres.2017.01.022.

[18] A.C.M. Franken, J.A.M. Nolten, M.H. V Mulder, D. Bargeman, C.A. Smolders, Wetting criteria for the applicability of membrane distillation, J. Memb. Sci. 33 (1987) 315–328. doi:10.1016/S0376-7388(00)80288-4.

[19] M. Rezaei, D.M. Warsinger, J.H. Lienhard V, W.M. Samhaber, Wetting prevention in membrane distillation through superhydrophobicity and recharging an air layer on the membrane surface, J. Memb. Sci. 530 (2017) 42–52. doi:10.1016/j.memsci.2017.02.013.

[20] S. Lin, S. Nejati, C. Boo, Y. Hu, C.O. Osuji, M. Elimelech, Omniphobic Membrane for Robust Membrane Distillation, Environ. Sci. Technol. Lett. 1 (2014) 443–447. doi:10.1021/ez500267p.

[21] G. Naidu, S. Jeong, S.J. Kim, I.S. Kim, S. Vigneswaran, Organic fouling behavior in direct contact membrane distillation, Desalination. 347 (2014) 230–239. doi:10.1016/j.desal.2014.05.045.

[22] C. Boo, J. Lee, M. Elimelech, Omniphobic Polyvinylidene Fluoride (PVDF) Membrane for Desalination of Shale Gas Produced Water by Membrane Distillation, Environ. Sci.

Technol. 50 (2016) 12275–12282. doi:10.1021/acs.est.6b03882.
[23] C. Boo, J. Lee, M. Elimelech, Engineering Surface Energy and Nanostructure of Microporous Films for Expanded Membrane Distillation Applications, Environ. Sci. Technol. 50 (2016) 8112–8119. doi:10.1021/acs.est.6b02316.
[24] Y.C. Woo, Y. Chen, L.D. Tijing, S. Phuntsho, T. He, J.S. Choi, et al., CF4plasma-modified omniphobic electrospun nanofiber membrane for produced water brine treatment by membrane distillation, J. Memb. Sci. 529 (2017) 234–242. doi:10.1016/j.memsci.2017.01.063.
[25] P. Peng, A.G. Fane, X. Li, Desalination by membrane distillation adopting a hydrophilic membrane, Desalination. 173 (2005) 45–54. doi:10.1016/j.desal.2004.06.208.
[26] X. Yang, R. Wang, L. Shi, A.G. Fane, M. Debowski, Performance improvement of PVDF hollow fiber-based membrane distillation process, J. Memb. Sci. 369 (2011) 437–447. doi:10.1016/j.memsci.2010.12.020.
[27] D.M. Warsinger, A. Servi, S. Van Belleghem, J. Gonzalez, J. Swaminathan, J. Kharraz, et al., Combining air recharging and membrane superhydrophobicity for fouling prevention in membrane distillation, J. Memb. Sci. 505 (2016) 241–252. doi:10.1016/j.memsci.2016.01.018.
[28] A.C.M. Franken, J.A.M. Nolten, M.H.V. Mulder, D. Bargeman, C.A. Smolders, Wetting criteria for the applicability of membrane distillation, J. Memb. Sci. 33 (1987) 315–328. doi:10.1016/S0376-7388(00)80288-4.
[29] M.M.C. Garcia-Payo, M.A.M. Izquierdo-Gil, C. Fernandez-Pineda, Wetting Study of Hydrophobic Membranes via Liquid Entry Pressure Measurements with Aqueous Alcohol Solutions, J. Colloid Interface Sci. 230 (2000) 420–431. doi:10.1006/jcis.2000.7106.
[30] N.G.P. Chew, S. Zhao, C.H. Loh, N. Permogorov, R. Wang, Surfactant effects on water recovery from produced water via direct-contact membrane distillation, J. Memb. Sci. 528 (2017) 126–134. doi:10.1016/j.memsci.2017.01.024.
[31] Y. Chen, Z. Wang, K. Jennings, S. Lin, Probing Pore Wetting in Membrane Distillation using Impedance: Early Detection and Mechanism of Surfactant-induced Wetting, Environ. Sci. Technol. Lett. 4 (2017) 505–510. doi:10.1021/acs.estlett.7b00372.
[32] Z. Wang, Y. Chen, X. Sun, R. Duddu, S. Lin, Mechanism of Pore Wetting in Membrane Distillation with Alcohol vs. Surfactant, J. Memb. Sci. 559 (2018) 183–195. doi:10.1016/j.memsci.2018.04.045.
[33] V.M. Starov, S.A. Zhdanov, M.G. Velarde, Capillary imbibition of surfactant solutions in porous media and thin capillaries: Partial wetting case, J. Colloid Interface Sci. 273 (2004) 589–595. doi:10.1016/j.jcis.2004.02.033.
[34] N.V. Churaev, G.A. Martynov, V.M. Starov, Z.M. Zorin, Some features of capillary imbibition of surfactant solutions, Colloid Polym. Sci. 259 (1981) 747–752.
[35] M.S. El-Bourawi, Z. Ding, R. Ma, M. Khayet, A framework for better understanding membrane distillation separation process, J. Memb. Sci. 285 (2006) 4–29. doi:10.1016/j.memsci.2006.08.002.
[36] M. Khayet, Membranes and theoretical modeling of membrane distillation: A review, Adv. Colloid Interface Sci. 164 (2011) 56–88. doi:10.1016/j.cis.2010.09.005.
[37] Y.G. Zmievskii, Determination of critical pressure in membrane distillation process, Pet. Chem. 55 (2015) 308–314. doi:10.1134/S0965544115040118.
[38] M.C. García-Payo, M.A. Izquierdo-Gil, C. Fernández-Pineda, Wetting study of hydrophobic membranes via liquid entry pressure measurements with aqueous alcohol

solutions, J. Colloid Interface Sci. 230 (2000) 420–431. doi:http://dx.doi.org/10.1006/jcis.2000.7106.
[39] D.E.M. Warsinger, A. Servi, G.B. Connors, M.O. Mavukkandy, H.A. Arafat, K. Gleason, et al., Reversing membrane wetting in membrane distillation: comparing dryout to backwashing with pressurized air, Environ. Sci. Water Res. Technol. 3 (2017) 930–939. doi:10.1039/C7EW00085E.
[40] . ar t nez-D ez .. V zquez -González, Temperature and concentration polarization in membrane distillation of aqueous salt solutions, J. Memb. Sci. 156 (1999) 265–273. doi:10.1016/S0376-7388(98)00349-4.
[41] R.W. Schofield, A.G. Fane, C.J.D. Fell, R. Macoun, Factors affecting flux in membrane distillation, Desalination. 77 (1990) 279–294. doi:10.1016/0011-9164(90)85030-E.
[42] N. Mikati, S. Wall, Diffusion of Sodium Dodecyl Sulfate Studied by a Steady-State Technique, Langmuir. 9 (1993) 113–116. doi:10.1021/la00025a026.
[43] M. Sudoh, K. Takuwa, H. Iizuka, K. Nagamatsuya, Effects of thermal and concentration boundary layers on vapor permeation in membrane distillation of aqueous lithium bromide solution, J. Memb. Sci. 131 (1997) 1–7. doi:10.1016/S0376-7388(97)00109-9.
[44] C.H. Chang, E.I. Franses, Adsorption dynamics of surfactants at the air/water interface: a critical review of mathematical models, data, and mechanisms, Colloids Surfaces A Physicochem. Eng. Asp. 100 (1995) 1–45. doi:10.1016/0927-7757(94)03061-4.
[45] J.R. McCutcheon, M. Elimelech, Influence of concentrative and dilutive internal concentration polarization on flux behavior in forward osmosis, J. Memb. Sci. 284 (2006) 237–247. doi:10.1016/j.memsci.2006.07.049.
[46] G.T. Gray, J.R. McCutcheon, M. Elimelech, Internal concentration polarization in forward osmosis: role of membrane orientation, Desalination. 197 (2006) 1–8. doi:10.1016/j.desal.2006.02.003.
[47] M.C. Porter, Concentration Polarization with Membrane Ultrafiltration, Ind. Eng. Chem. Prod. Res. Dev. 11 (1972) 234–248. doi:10.1021/i360043a002.
[48] J. Zhang, N. Dow, M. Duke, E. Ostarcevic, J.D. Li, S. Gray, Identification of material and physical features of membrane distillation membranes for high performance desalination, J. Memb. Sci. 349 (2010) 295–303. doi:10.1016/j.memsci.2009.11.056.
[49] K. Smolder, A. Franken, Terminology for Membrane Distillation, Desalination. 72 (1989) 249–262.
[50] Y.X. Huang, Z. Wang, J. Jin, S. Lin, Novel Janus Membrane for Membrane Distillation with Simultaneous Fouling and Wetting Resistance, Environ. Sci. Technol. 51 (2017) 13304–13310. doi:10.1021/acs.est.7b02848.
[51] D. Hou, Z. Wang, K. Wang, J. Wang, S. Lin, Composite membrane with electrospun multiscale-textured surface for robust oil-fouling resistance in membrane distillation, J. Memb. Sci. 546 (2018) 179–187. doi:10.1016/j.memsci.2017.10.017.
[52] Y. Kwon, N. Patankar, J. Choi, J. Lee, Design of surface hierarchy for extreme hydrophobicity, Langmuir. 25 (2009) 6129–6136. doi:10.1021/la803249t.
[53] Z. Wang, M. Elimelech, S. Lin, Environmental Applications of Interfacial Materials with Special Wettability, Environ. Sci. Technol. 50 (2016) 2132–3150.
[54] M.S. Romero-Cano, A. Martín-Rodríguez, F.J. de las Nieves, Adsorption and Desorption of Triton X-100 in Polystyrene Particles with Different Functionality: I. Adsorption Study, J. Colloid Interface Sci. 227 (2000) 322–328. doi:http://dx.doi.org/10.1006/jcis.2000.6862.
[55] H.H. Paradies, Shape and size of a nonionic surfactant micelle. Triton X-100 in aqueous

solution, J. Phys. Chem. 84 (1980) 599–607. doi:10.1021/j100443a008.
[56] Z. Adamczyk G. Para P. Warszyński Influence of ionic strength on surface tension of cetyltrimethylammonium bromide, Langmuir. 15 (1999) 8383–8387. doi:10.1021/la990241o.
[57] A.B. Mandal, B.U. Nair, Cyclic voltammetric technique for the determination of the critical micelle concentration of surfactants, self-diffusion coefficient of micelles, and partition coefficient of an electrochemical probe, J. Phys. Chem. 95 (1991) 9008–9013. doi:10.1021/j100175a106.
[58] C.H. Chang, E.I. Franses, Modified Langmuir-Hinselwood kinetics for dynamic adsorption of surfactants at the air/water interface, Colloids and Surfaces. 69 (1992) 189–201. doi:10.1016/0166-6622(92)80230-Y.

Highlights

- We developed a kinetic model for pore wetting induced by surfactants;
- The model accounts for convection, diffusion, and adsorption of surfactants;
- Kinetics of pore wetting mostly depends on how fast the pore surface is saturated;
- Surfactant concentration and vapor both have strong impact on wetting kinetics;
- Transmembrane hydraulic pressure has little impact on pore wetting kinetics;